High-Fidelity Low-Earth Orbit Collision Avoidance Trajectories using bang-bang optimal control laws

IAC-24-A6.IP.82.x89038

High-Fidelity Low-Earth Orbit Collision Avoidance Trajectories using bang-bang optimal control laws

Sarcletti G.[a], Mascolo L. [a], Battipede M [a].

[a] *Department of Mechanics and Aerospace, Politecnico di Torino, Torino Italy*

Abstract

The ever-increasing density of objects in low Earth orbit (LEO) has raised concerns about the potential for a future cascade of collisions, a phenomenon known as the Kessler Syndrome. Such collisions could inflate the amount of space debris, posing significant risks to operational satellites and future space missions. In response to this, and in alignment with new de-orbit regulations, there is a shift towards refining collision avoidance strategies to minimize propellant consumption. Indeed, despite the relatively low fuel requirements of individual collision avoidance maneuvers, their growing necessity places a considerable strain on satellite fuel budgets. In this context, the objective of this research is to develop a tool that uses indirect optimization to identify propellant-efficient collision avoidance trajectories between two orbiting objects. To this end, the indirect approach is employed to exploit the theory of optimal control, applied to spacecraft trajectories, and to transform the optimization problem into a boundary value problem, which is subsequently solved by means of shooting procedures. This method ensures precise optimization and offers significant advantages in terms of computational costs, particularly when low-thrust is considered. Trajectory optimization is performed using a simple two-body dynamic model. This approach ensures robust convergence of the optimization method and maintains dynamic accuracy, due to the low maneuvering times involved.

Keywords: optimization, indirect, LEO, CAM, low-thrust

1. Introduction

Trajectory analysis and optimization is crucial to the success or even feasibility of a space mission. The problem can be stated as the determination of a trajectory that satisfies some constraints required by the mission, while extremizing some quantity of importance. Since the trajectory followed by a spacecraft directly impacts on the amount of propellant needed for set mission, hence influences the mass budget, which relates to mission feasibility and costs, the most common objective is to minimize propellant consumption or equivalently to maximize the spacecraft's final mass. Indirect methods use the optimal control theory (OCT) to derive first-order necessary conditions and transform the optimization problem into a boundary value problem (BVP), which is then solved, starting from a tentative solution, by means of shooting procedures. The most important feat of indirect methods is that they provide first order optimal solutions -in the limits of the dynamic model and the numerical accuracy of integration-. Moreover they offer low computational costs and vast theoretical insight over the optimization problem, but the necessity of deriving case-specific equations and defining near-optimal guesses have made these methods less appealing than the direct ones. The most suitable mathematical formulation for an optimization problem regarding finite-thrust missions is a time-continuous optimal control problem [1].

2. The Optimal Control Problem

An Optimal Control Problem (OCP) aims at maximizing a chosen merit index by establishing an admissible control law, while ensuring that the system satisfies specified constraints, as it evolves from an initial to a final state over a defined time interval.

The system is described by a set of state variables $x(t) \in \mathbb{R}^n$ that evolve over time according to n first order differential equations. These ODEs are function of the state vector x(t), the control vector $u(t) \in \mathbb{R}^m$, which contains the m control variables, and, of course, the independent variable time t. The ODE system can be generically written as:

$$\dot{\boldsymbol{x}}(t) = f\,(x(t), u(t), t) \qquad (2.1)$$

An optimal solution defines the optimal trajectory $\mathbf{x}^*(t)$, subject to optimal controls $\mathbf{u}^*(t)$, that maximizes a specified merit index. the optimal trajectory must satisfy constraints of various kind; if these constraints concern state and time solely at the extremes of the time interval, the problem defined in (2.1) is a Two Point Boundary Value Problem (TPBVP) and the extremal boundary conditions imposed at $t = t_0$ and at $t = t_f$ are called external boundaries. These BCs can be written as a set of homogeneous algebraic equations and grouped in the constraint vector:

$$\boldsymbol{\psi}(\boldsymbol{x_0}, \boldsymbol{x_f}, t_0, t_f) = \mathbf{0} \qquad (2.2)$$

where $\boldsymbol{\psi} : [\mathbb{R}^n, \mathbb{R}^n, \mathbb{R}, \mathbb{R}] \rightarrow \mathbb{R}^q$ collects the q constraints; x_0 and $\mathbf{x}_f$ stand for $\mathbf{x}(t_0)$ and $\mathbf{x}(t_f)$ respectively. Constraints

may also concern the control variables u, therefore u ∈ U, where U represents the set of admissible controls.
The criterion that completes the OCP and drives the optimization process is represented by the merit (or performance) index J, which must be maximized or minimized. In general, J is a functional comprised of two terms:

$$J = \varphi(\boldsymbol{x_0}, \boldsymbol{x_f}, t_0, t_f) + \int_{t_0}^{t_f} [\Phi(\boldsymbol{x}(t), \boldsymbol{u}(t), t)]dt \qquad (2.3)$$

where the first function φ depends uniquely on the values assumed by the state and time variables at the boundaries, and the second term depends on the values that the state variables, controls and time assume during the trajectory. Equation (2.3) can be equivalently rewritten in Lagrange's or in Mayer's formulation, respectively by posing φ = 0 or Φ = 0 and by introducing opportune auxiliary variables. Mayer's formulation is usually preferred to define an optimization problem that searches for extremal values of a functional, which is the case of this work's OCP.

2.1 Necessary Conditions

A necessary, or first order, condition for optimality dictates that the first variation of the performance index J must be zero for any permissible variation along the trajectory and at the boundaries [2]. A modified functional, or augmented merit index, J^* is defined through the introduction of Lagrange multipliers μ and adjoint variables λ [3].
The modified functional in Mayer's formulation is defined as:

$$J^* = \varphi + \boldsymbol{\mu^T \psi} + \int_{t_i}^{t_f} [\boldsymbol{\lambda^T} (\boldsymbol{f} - \dot{\boldsymbol{x}})]\, dt \qquad (2.4)$$

$J^* = J$ if $\boldsymbol{\psi} = \mathbf{0}$ and $\boldsymbol{f} - \dot{\boldsymbol{x}} = \mathbf{0}$, that is if all boundary conditions and differential equations are respected, therefore, solving the augmented problem with the modified functional in equation (2.4) is mathematically equivalent to solving the problem with the original functional defined in (2.3), provided all constraints are respected.
By differentiating J^* it is possible to distinguish five different terms which, set to zero, give 2 transversality conditions on time, 2n optimality conditions regarding the state, n Euler-Lagrange conditions for the adjoint variables and m algebraic equations for the control variables. Moreover, an important quantity defined as the system's Hamiltonian, H, can be identified:

$$H \triangleq \boldsymbol{\lambda^T f} \qquad (2.5)$$

The optimal control $\boldsymbol{u}^* \in \mathbf{U}$ for the optimal trajectory is the one that maximizes the Hamiltonian in each point of the trajectory. This concept is known as Pontryagin's Maximum Principle (PMP) [4].

3. Numerical Methods for Indirect Optimization

The most well-known methods to solve the BVP numerically are the shooting techniques; collocation methods are also exploited to solve generic BVPs. Besides these general-purpose methods, a sequential gradient restoration algorithm can be implemented to solve BVPs that originate from OCPs. Due to their straight-forward implementation and high efficiency, shooting techniques are the implemented numerical method to solve the BVPs in this work.

3.1 Single Shooting

Shooting methods transform the Boundary Value Problem into an Initial Value Problem (IVP), which can be solved via well-established algorithms and led to convergence by Newton-like or gradient methods. They are easy to understand and very efficient, but their efficacy is strongly linked to the behaviour of the IVP [5]. Starting from an initial guess, initial conditions are adjusted exploiting Newton-like or gradient based methods through a process of differential correction. Hence, the BVP that describes a trajectory optimization problem is transformed into an Initial Value Problem (IVP), which is iteratively solved via numerical integration to compute corrections (through a differential corrector) for undesired terminal deviation, updating the initial conditions at each r-th iteration.

3.2 Differential Correction

The differential correction procedure aims at nullifying the difference between the desired final state and costate vector $\boldsymbol{y}_f^*$ and the one obtained via IVP resolution $\boldsymbol{y}_f$. Let $\delta\boldsymbol{y}_f$ be the discrepancy between the desired and the actual final vectors:

$$\delta\mathbf{y}_f = \mathbf{y}(\mathbf{y}_0, t_f) - \mathbf{y}^*(\mathbf{y}_0^*, t_f) \qquad (3.1)$$

A specific correction in the initial state, say $\delta\boldsymbol{y}_0$, should produce the needed initial state $\boldsymbol{y}_0^*$:

$$\boldsymbol{y}_0^* = \boldsymbol{y}_0 + \delta\boldsymbol{y}_0 \qquad (3.2)$$

A first order Taylor expansion of the constraint vector $\boldsymbol{\psi}$ is performed to evaluate how to update the initial state.

The derivatives of the constraints with respect to the state vector quantities form a Jacobian matrix $\boldsymbol{G}(\boldsymbol{\psi}(\boldsymbol{y}_0), \boldsymbol{y}) \in \mathbb{R}^{q\times 2n}$ that can be referred to as Error Gradient Matrix:

$$\boldsymbol{G}(\boldsymbol{\psi}(\mathbf{y}_0), \mathbf{y}) = \frac{\partial \boldsymbol{\psi}(\mathbf{y_0})}{\partial \mathbf{y}} = \begin{pmatrix} \frac{\partial \psi_1}{\partial y_1} & \frac{\partial \psi_1}{\partial y_2} & \cdots & \frac{\partial \psi_1}{\partial y_{2n}} \\ \frac{\partial \psi_2}{\partial y_1} & \frac{\partial \psi_2}{\partial y_2} & \cdots & \frac{\partial \psi_2}{\partial y_{2n}} \\ \vdots & \vdots & \ddots & \vdots \\ \frac{\partial \psi_q}{\partial y_1} & \frac{\partial \psi_q}{\partial y_2} & \cdots & \frac{\partial \psi_q}{\partial y_{2n}} \end{pmatrix} \quad (3.3)$$

The error gradient matrix linearly maps the variation of the errors on the boundary conditions to the variations of the initial state. It can be obtained analytically, but this procedure is usually rather heavy both in terms of analytical effort to obtain the necessary equations, and time to program and debug the code. Thus, the analytical approach should be employed only when other numerical techniques fail to provide convergence. In this work a numerical method is adopted.

3.3 Newton's Method

The values of the error gradient matrix G are obtained by varying the unknowns by a small amount and solving the IVP with the new perturbed initial conditions vector. The correction of the tentative values is thus obtained under a linear approximation.

Let r represent the current step of the iterative shooting procedure: $(\mathbf{y}_0)_r$ is perturbed by a small delta in its i-th component in order to obtain the error gradient matrix's i-th column. According to a forward-finite-difference scheme: Let $[(\mathbf{y}_0)_r]_p$ be the perturbed initial state:

$$[(\boldsymbol{y}_0)_r]_p = (\boldsymbol{y}_0)_r + \boldsymbol{e}_i \cdot \Delta \quad (3.4)$$

where $\mathbf{e}_i$ is a 2n-component-unit-vector, with all elements equal to zero except for the i-th element. Then the i-th column of the error gradient matrix is:

$$\boldsymbol{G}_r[:, i] = \frac{[(\boldsymbol{\psi}(\boldsymbol{y}_0))_r]_p - (\boldsymbol{\psi}(\boldsymbol{y}_0))_r}{\Delta} \quad (3.5)$$

The r+1 initial guess is then defined as:

$$(\boldsymbol{y}_0)_{r+1} = (\boldsymbol{y}_0)_r - \boldsymbol{G}_r^{-1}(\boldsymbol{\psi}((\boldsymbol{y}_0))_r \quad (3.6)$$

Linearization may introduce errors that can prevent convergence and induce instability; for this reason two relaxation parameters are introduced, K_1 and K_2. Both reduce the parameter correction: K_1 is utilized performing a check on error variation and reducing, usually by half, parameter correction if $\max(\boldsymbol{\psi}_{r+1}) > K_1\max(\boldsymbol{\psi}_r)$. This operation is known as bisection; the bisection parameter K_1 is usually equal to 2. K_2 is introduced in the correction scheme:

$$(\boldsymbol{y}_0)_{r+1} = (\boldsymbol{y}_0)_r - K_2\boldsymbol{G}_r^{-1}(\boldsymbol{\psi}((\boldsymbol{y}_0))_r \quad (3.6)$$

K_2 is usually set in the range $0.01 \leq K_2 \leq 1$ but its efficacy is strongly dependent on the closeness of the initial state to the actual solution and on the overall problem dimensions. The closer to the solution, the greater K_2 can be.

4. Dynamic Model

A simple Two Body Problem (2BP) was implemented to allow for easier convergence and faster computation time. This choice is justified by the order of magnitude of the accelerations involved in the LEO environment: Earth's gravitational pull is by far the strongest, with an order of magnitude between $1x10^{-2}$ and $1x10^{-3}$ km/s, whilst other celestial bodies like the Sun and Moon cause accelerations of around $1x10^{-9}$ km/s. Drag is the strongest perturbation at lower altitudes but is highly dependent on the analyzed object's attitude and consequent reference surface, with accelerations varying between $1x10^{-5}$ and $1x10^{-12}$ km/s within the first km above Earth surface. Earth oblateness, represented by the J2 coefficient causes a deviation of the gravitational field of Earth from perfect sphere with an acceleration of around $1x10^{-5}$. In first approximation and with restrained propagation times it is possible to neglect these perturbations.

5. The Implemented OCP

The OCP applied to the system of ODEs derived for a two-body dynamic model in the J2000 reference frame (J2000 RF) aims to find the optimal control law $\boldsymbol{T}^*(t)$ that maximizes the final mass of the spacecraft at the end of the trajectory and is defined as:

$$OCP = \begin{cases} max\ J = m_f \\ \begin{cases} \dot{\boldsymbol{r}}(t) = \boldsymbol{V}, & t \in [0, tf\,] \\ \dot{\boldsymbol{V}}(t) = -\frac{\mu}{r^3}\boldsymbol{r} + \frac{\boldsymbol{T}}{m(t)}, & t \in [0, tf\,] \\ \dot{m}(t) = -\frac{T}{c}, & t \in [0, tf\,] \end{cases} \\ s.t. \\ T \leq T_{max} \\ \boldsymbol{r}_i, \boldsymbol{V}_i \leftarrow initial\ orbit\ keplerian\ elements \\ \boldsymbol{r}_f, \boldsymbol{V}_f \leftarrow target\ orbit\ keplerian\ elements \\ m_i = m_{sc} \\ t_f = free \end{cases} \quad (5.1)$$

To each state variable is associated a costate, or adjoint, variable. The augmented state vector, or fullstate, is defined as:

$$\begin{aligned} \boldsymbol{fullstate} &= \{x, y, z, v_x, v_y, v_z, m, \lambda_x, \lambda_y, \lambda_z, \lambda_{vx}, \\ &\quad \lambda_{vy}, \lambda_{vz}, \lambda_m\} \\ &= \{\boldsymbol{r}, \boldsymbol{V}, m, \boldsymbol{\lambda_r}, \boldsymbol{\lambda_V}, \lambda_m\} = \{\boldsymbol{S}, m, \boldsymbol{C}, \lambda_m\} \end{aligned} \quad (5.2)$$

Now the Hamiltonian for the defined OCP can be obtained:

$$\begin{aligned} H &= \boldsymbol{\lambda}^T \boldsymbol{f} \\ &= \boldsymbol{\lambda_r} \cdot \boldsymbol{V} + (\boldsymbol{\lambda_V} \cdot \boldsymbol{r})\frac{-\mu}{r^3} + \boldsymbol{\lambda_V} \cdot \frac{\boldsymbol{T}}{m} - \lambda_m \frac{T}{c} \end{aligned} \quad (5.3)$$

5.1 Optimal Thrust

The PMP states that the optimal control maximizes the Hamiltonian H in order to maximize the merit index *J*. As it can be seen from equation (5.3), the optimal thrust direction that maximizes the Hamiltonian is parallel to the adjoint velocity vector, or primer vector, λ_V:

$$\boldsymbol{T} = T\frac{\boldsymbol{\lambda_V}}{\lambda_V} \tag{5.4}$$

where λ_V is the primer vector's module:

$$\lambda_V = \sqrt{\lambda_{vx}^2 + \lambda_{vy}^2 + \lambda_{vz}^2} \tag{5.5}$$

The thrust vector can be decomposed as in Fig. 1.:

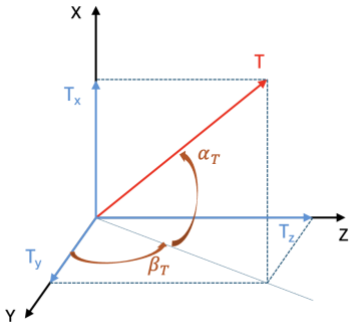

Fig. 1. Thrust angles in the cartesian RF

with:

$$\begin{cases} T_x = T\ \sin\alpha_T \\ T_y = T\ \cos\alpha_T\ \cos\beta_T \\ T_z = T\ \cos\alpha_T\ \sin\beta_T \end{cases} \tag{5.6}$$

Hence, the thrust angles α_T and β_T can be expressed in terms of the velocity costates:

$$\begin{aligned} \sin\alpha_T &= \frac{\lambda_{vx}}{\lambda_V} \\ \cos\alpha_T\ \cos\beta_T &= \frac{\lambda_{vy}}{\lambda_V} \\ \cos\alpha_T\ \sin\beta_T &= \frac{\lambda_{vz}}{\lambda_V} \end{aligned} \tag{5.7}$$

By grouping the terms that contain the control variable T in equation (5.3), the Hamiltonian can be re-written by highlighting the switching function, SF:

$$H = \boldsymbol{\lambda_r}\cdot\boldsymbol{V} + (\boldsymbol{\lambda_V}\cdot\boldsymbol{r})\frac{-\mu}{r^3} + T\ SF \tag{5.8}$$

$$SF = \frac{\lambda_V}{m} - \frac{\lambda_m}{c} \tag{5.9}$$

From equation (5.8) it is clear that the Hamiltonian is linear with the control: a bang-bang control law arises, so that the optimal thrust magnitude is maximized when its multiplier, the switching function, is positive, and is minimized when the SF is negative:

$$T = \begin{cases} T_{max} & if\ SF > 0 \\ 0 & if\ SF < 0 \end{cases} \tag{5.10}$$

5.2 Euler-Lagrange Equations

The ODEs for the costate variables are obtained via the partial derivation of the Hamiltonian with respect to the corresponding state variables, with a minus sign; the resulting vectorial equations are here reported:

$$\frac{d\boldsymbol{\lambda_r}}{dt} = -\frac{\partial \boldsymbol{g}}{\partial \boldsymbol{r}}\cdot\boldsymbol{\lambda_V} \tag{5.11a}$$

$$\frac{d\boldsymbol{\lambda_V}}{dt} = -\boldsymbol{\lambda_r} \tag{5.11b}$$

$$\frac{d\lambda_m}{dt} = \frac{T}{m^2}\lambda_V \tag{5.11c}$$

where in equation (5.11a) $\boldsymbol{g} = -\frac{\mu}{r^3}\boldsymbol{r}$.

5.3 Terminal Conditions

The maneuver of choice in this work is a free-time (time isn't constrained), free-attachment orbital insertion. A free-attachment orbital insertion doesn't specify the insertion point on the final orbit, leaving the final true anomaly as a free variable, to be determined by the optimal solution. For this purpose, the reduced transversality conditions described in [6] were exploited to obtain a condition that accounts for the added degree of freedom of the true anomaly. The reduced transversality conditions are analogous to the transversality conditions,
here referred to as "optimality conditions", for the same OCP, with the variables in the terminal constraints replaced by the orbital elements.
A solution for a free-time, free-attachment orbital insertion must include the seven initial costates, the time to maneuver and the final true anomaly. Nine total unknowns require 9 boundary conditions:

- Maximum final mass:

$$\lambda_{mf} = 1 \tag{5.12}$$

- Unconstrained time to maneuver:

$$H_f = 0 \tag{5.13}$$

- Free-attachment orbital insertion:

$$\boldsymbol{V_f}\cdot\boldsymbol{\lambda_{rf}} - \frac{\mu}{r_f^3}\boldsymbol{r_f}\cdot\boldsymbol{\lambda_{Vf}} = 0 \tag{5.14}$$

- Final state BCs:

$$\boldsymbol{r_f} = \boldsymbol{r_f^*} \tag{5.15a}$$

$$\boldsymbol{V_f} = \boldsymbol{V_f^*} \tag{5.15b}$$

where $\boldsymbol{r}_f^*$ and $\boldsymbol{V}_f^*$ represent the final desired state, which is obtained by updating the required final Keplerian elements with a new final true anomaly in every new iteration.

5.4 Differential Correction - Jacobian Matrix

The Jacobian matrix is calculated iteratively by column, by perturbing each guess solution (the seven costates, the true anomaly and the time of maneuver) of a Δ, which is usually the same for every variable. Notice that when perturbing the final true anomaly, no integration of the system's ODEs is required since no initial value is perturbed in the IVP. This was the reason why it was opted to perform Point-to-Orbit maneuvers and not vice versa. (5.16) displays how the Jacobian matrix involved in this work is composed.

$$G = \begin{pmatrix} \frac{(\delta x_f)_p - \delta x_f}{\Delta_{\lambda x}} & \frac{(\delta x_f)_p - \delta x_f}{\Delta_{\lambda y}} & \cdots & \frac{(\delta x_f)_p - \delta x_f}{\Delta_\nu} & \frac{(\delta x_f)_p - \delta x_f}{\Delta_t} \\ \vdots & \vdots & \ddots & \vdots & \\ \frac{(\delta \lambda_{mf})_p - \delta \lambda_{mf}}{\Delta_{\lambda x}} & \frac{(\delta \lambda_{mf})_p - \delta \lambda_{mf}}{\Delta_{\lambda y}} & \cdots & \frac{(\delta \lambda_{mf})_p - \delta \lambda_{mf}}{\Delta_\nu} & \frac{(\delta \lambda_{mf})_p - \delta \lambda_{mf}}{\Delta_t} \\ \frac{(\text{free}\nu)_p - \text{free}\nu}{\Delta_{\lambda x}} & \frac{(\text{free}\nu)_p - \text{free}\nu}{\Delta_{\lambda y}} & \cdots & \frac{(\text{free}\nu)_p - \text{free}\nu}{\Delta_\nu} & \frac{(\text{free}\nu)_p - \text{free}\nu}{\Delta_t} \\ \frac{(H_f)_p - H_f}{\Delta_{\lambda x}} & \frac{(H_f)_p - H_f}{\Delta_{\lambda y}} & \cdots & \frac{(H_f)_p - H_f}{\Delta_\nu} & \frac{(H_f)_p - H_f}{\Delta_t} \end{pmatrix} \quad (5.16)$$

6. Case Study

Collision avoidance maneuvers (CAMs) could be performed by changing any orbital element of at least one of the colliding objects, but in-track maneuvers are usually the preferred strategy, since a change in the semimajor axis directly affects the radial distance between the satellites and affects the orbital period; the distance at closest approach is increased by the combined effect of these 2 phenomena, while ΔV requirements are minimized. Therefore, Δa maneuvers are investigated, under the hypothesis of a free-attachment orbital insertion, unconstrained in terms of time.

6.1 Boundary Conditions and Problem Hypotheses

In order to simulate an actual scenario, the primary spacecraft's propulsion characteristics were based on a datasheet from state-of-the-art Hall-effect thrusters suitable for use as main propulsors in small-sized satellites. The case study is set in the lower region of the LEO environment, which is the typical operational domain for these kinds of spacecraft.

Two objects of interest were modeled in a developed tool designed to compute the probability of collision (PoC), with the following Keplerian elements:

	a[km]	*e[deg]*	*i[deg]*	*Ω[deg]*	*ω[deg]*	*ν[deg]*
Primary	*6678.000*	*0.00*	*45.00*	*1.00*	*0.00*	*1.00*
Secondary	*6678.115*	*0.00*	*−0.01*	*0.00*	*0.00*	*0.99*

Table 1. Example satellites' Keplerian parameters

Traditionally, in close approach analysis, the spacecraft responsible of performing the evasion maneuver is referred to as "primary", whereas the other spacecraft (or debris) involved is called "secondary".

For the purposes of this illustrative example, both objects have initial circular orbits and the same geometric and mass properties:

$$r_{sat-p} = r_{sat-s} = 1m \quad (6.1a)$$

$$m_{sat-p} = m_{sat-s} = 150kg \quad (6.1b)$$

The primary spacecraft has a Hall-effect thruster with the following specifications:

$$Isp = 1400s, \quad T = 0.025N$$

The PoC computation tool yields the following predicted conjunction event:

TCA [s]	***d_{close} [km]***	***PoC***
10818.04	*0.107284*	*3.614×10^{-4}*

Table 2. Predicted conjunction event

where TCA is the time of closest approach and d_{close} is the minimum distance between the two objects (at TCA). According to the safety standards defined by ESA [7]. A collision avoidance maneuver is hereby required.

6.2 Maneuver definition

By iteratively searching for an evasion orbit for the primary spacecraft that guarantees safety (PoC < 1×10^{-4}) during the conjunction event, the least propellant demanding maneuver is found to be a semimajor axis lowering of 19 meters. The evasion maneuver yields the following results:

TCA [s]	***d_{close} [km]***	***PoC***	***Δa [km]***	***m_p [kg]***	***t_{CAM} [s]***
10818.53	*0.388371*	*9.959×10^{-5}*	*-0.019*	*1.192×10^{-5}*	*667.76*

Table 3. Conjunction event after the CAM and CAM data

Fig. 2. summarizes the variation of the primary spacecraft's Keplerian elements during the evasion maneuver along with the switching function and optimal thrust angles.

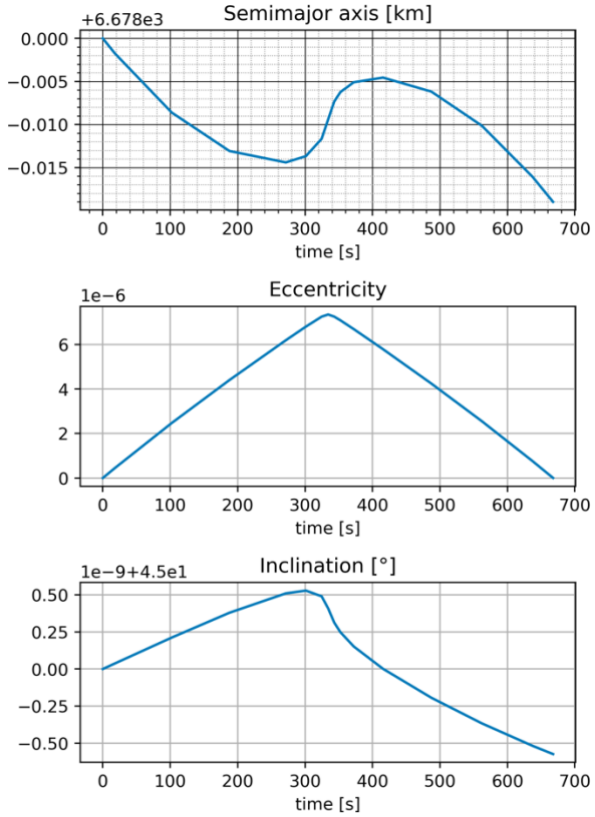

(a) Semimajor axis, eccentricity and inclination true anomaly during the maneuver

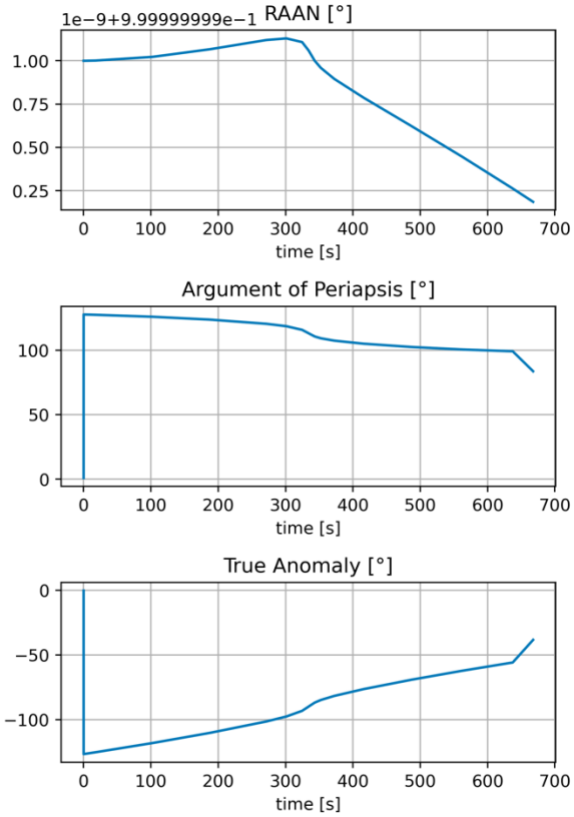

(b) RAAN, argument of periapsis and during the maneuver

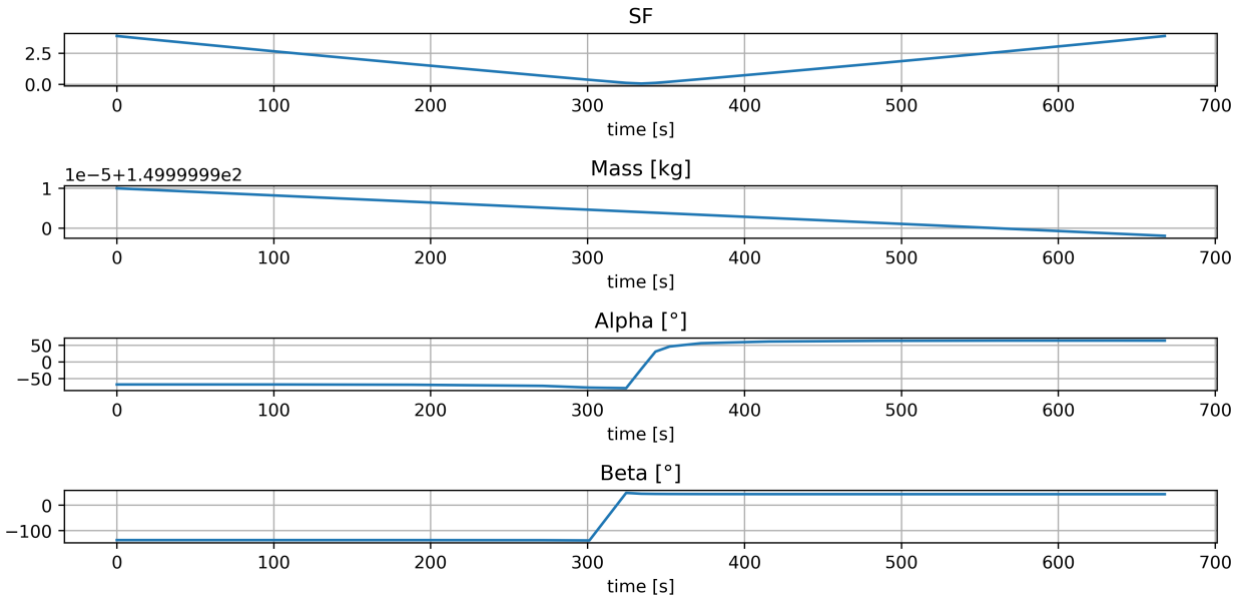

(c) Switching function, mass and thrust angles during the maneuver

Fig. 2. Evolution of spacecraft and control variables during the selected CAM

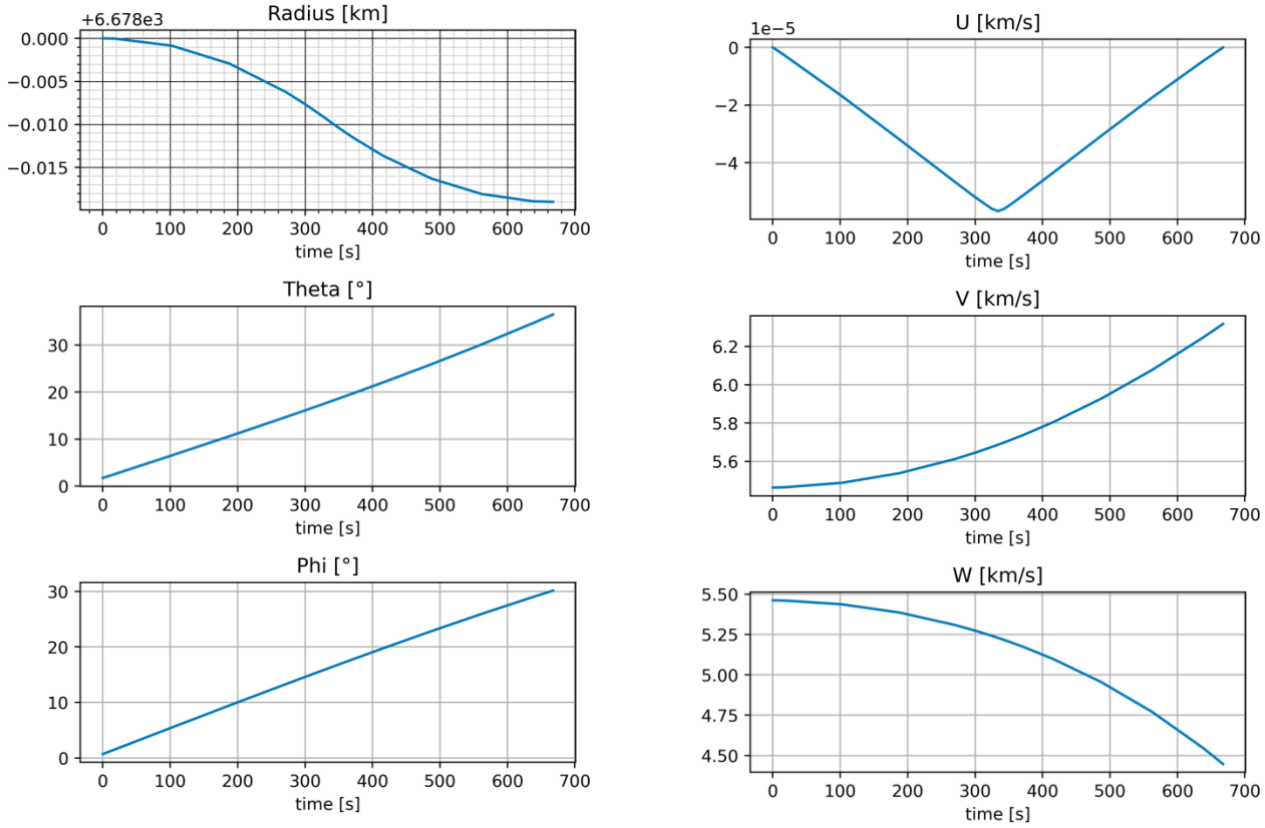

(a) J2000 polar coordinates

(b) ZEN velocities

Fig. 3. Evolution of spacecraft's state in J2000/ZEN coordinates during the selected CAM

The semimajor axis behavior during the identified maneuver can be misleading: by not being monotonically decreasing, it may induce the wrongful idea of the maneuver not being optimal for its case. As the J2000 polar coordinates in Fig. 3. clarify, the radius is in fact monotonically decreasing, while the semimajor axis isn't. This is a consequence of the eccentricity requirement, which dictates the circularization of the targeted orbits and therefore causes semimajor axis variation.

Note that the radial component of the velocity starts and ends at zero, confirming that the initial and final orbits are in fact circular, and the east and north components evolve along the trajectory according to the orbital plane's inclination: the closer to the ascending node ($\varphi = 0$), the higher the north component w is, and, the closer is the out-of-plane angle φ to the orbit's inclination, the higher the east velocity component v.

6.3 Parametric Analysis of results

In order to extrapolate additional useful insights from this example a parametric evaluation of the maneuver to be performed by the primary satellite was carried out with the trajectory optimization tool. Iteratively the tool evaluated a Hohmann-like maneuver with a target delta semimajor axis spanning between −50m and +50m. A constant $\Delta a = 10$m step was adopted to find the first solutions, using a continuity approach, additional solutions where found by setting $\Delta a = 5$ between the solutions that yielded the best results in terms of PoC. The following graphs highlight the evolutions of the solutions' keplerian parameters (Fig. 4. and Fig. 5.), polar J2000 positions (Fig. 6.) and ZEN velocities (Fig. 7.) as well as the controls and the spacecraft's mass (Fig. 8.):

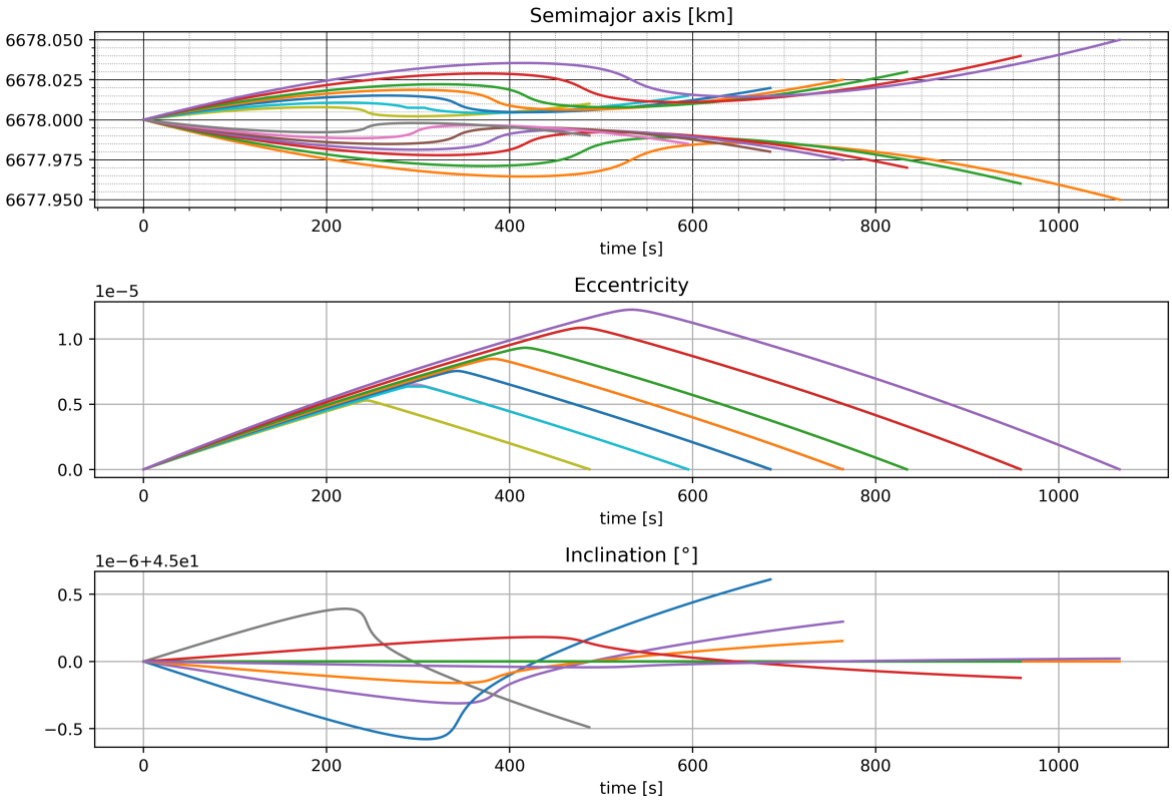

Fig. 4. Semimajor axis, eccentricity and inclination during the evaluated maneuvers

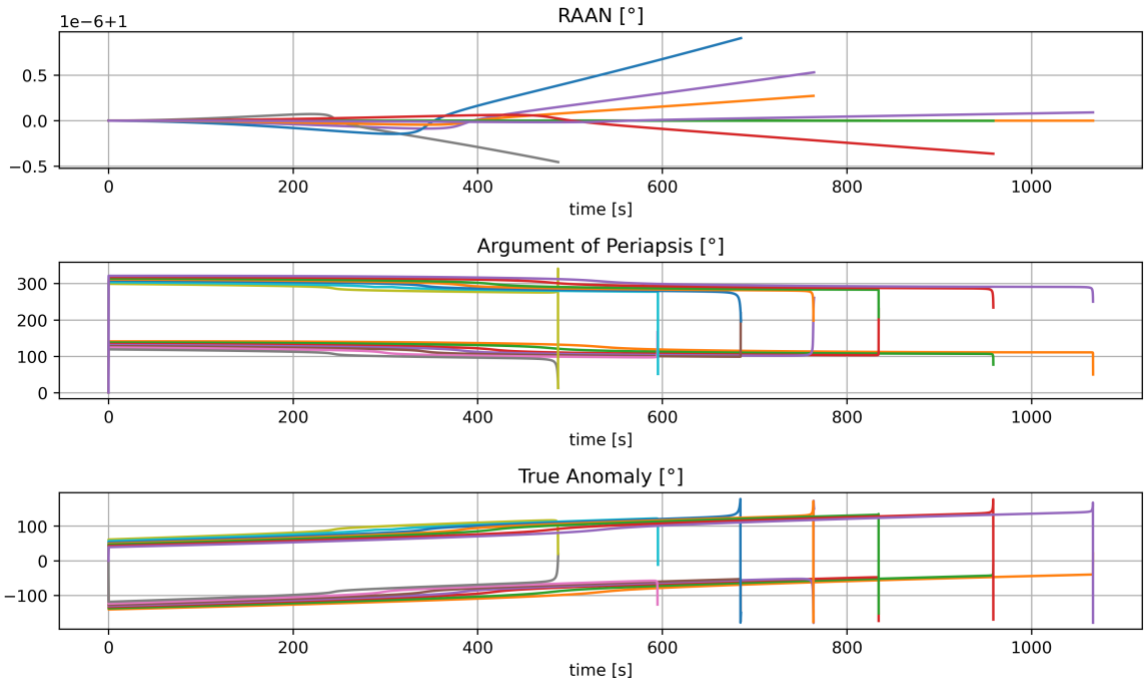

Fig. 5. RAAN, argument of periapsis and true anomaly during the evaluated maneuvers

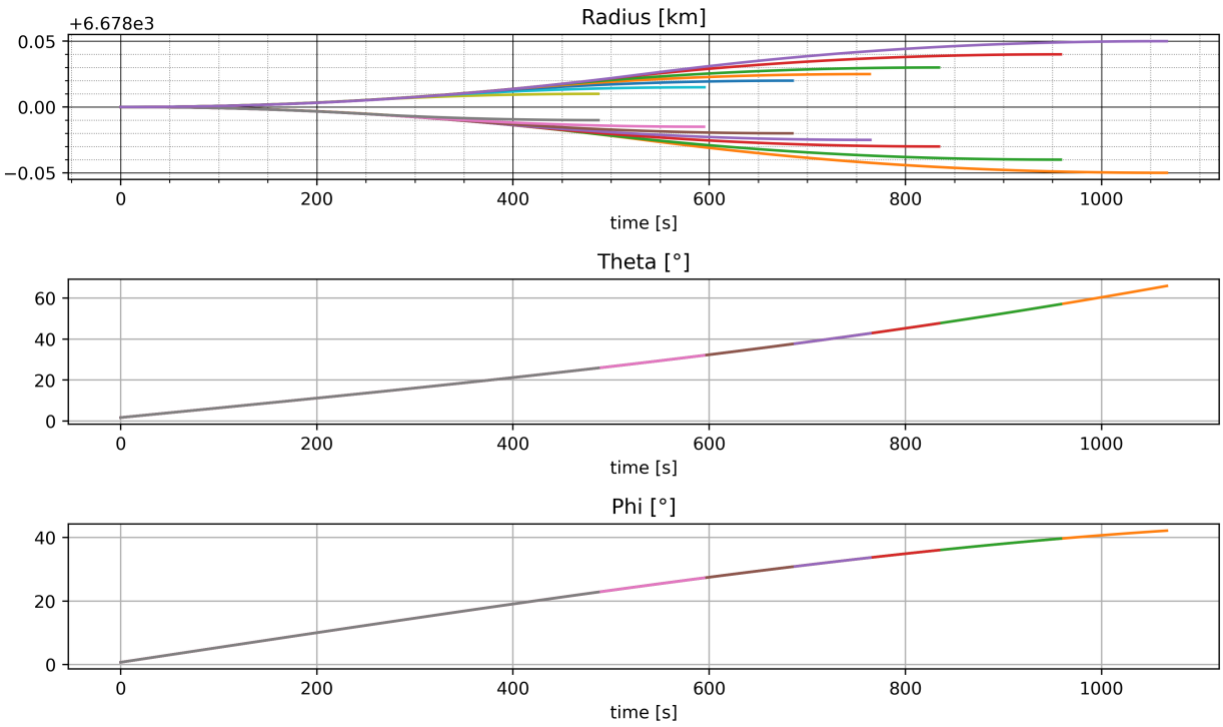

Fig. 6. J2000 Polar coordinates during the evaluated maneuvers

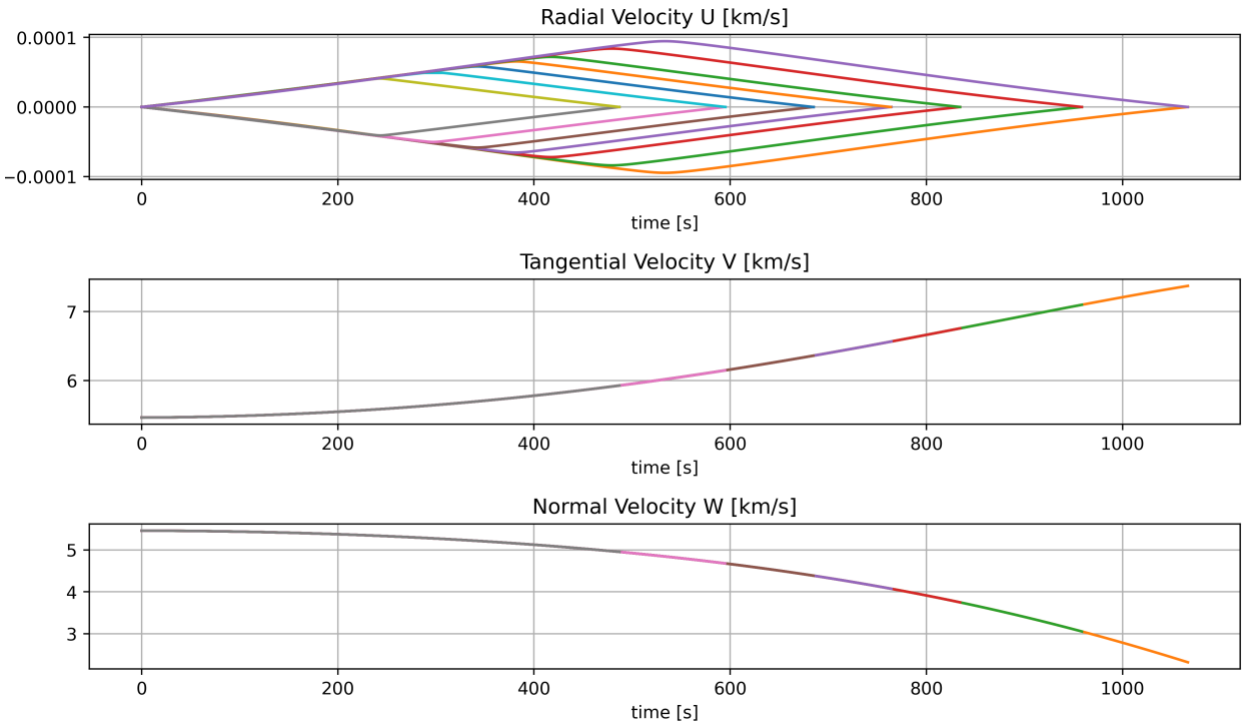

Fig. 7. ZEN velocities during the evaluated maneuvers

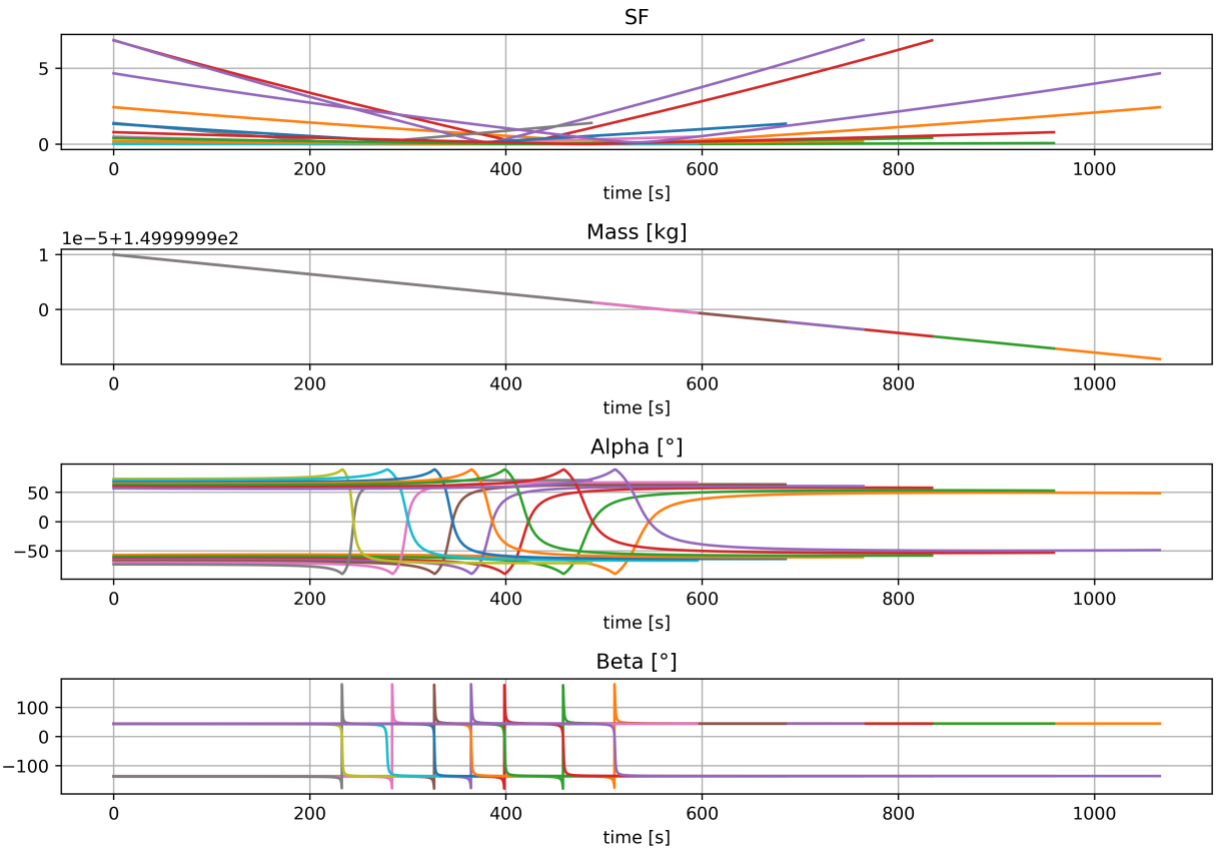

Fig. 8. Switching function, mass and thrust angles during the evaluated maneuver

As illustrated in the switching function graph (Fig. 8.), all solutions identified are characterized by the presence of continuous propulsion. The sole exception is the case of Δa = +15m, which exhibited a brief coasting phase (visible in the semimajor axis graph in Fig. 4., light blue line). The reasons for this behavior can be attributed to the extremely small state variations targeted, paired with a low-thrust control and, possibly, the lack of an a-priori arc definition. Furthermore, the time of maneuver was set to be free, but bounded to a maximum value of an orbital period, which precludes the possibility for the solution to have multiple thrusting arcs at perigees, where theoretically most efficient. This was an author's decision related to this trajectory optimization's objectives of providing short-term evasion maneuvers, and that certainly helped in obtaining convergence by reducing the solution search space. Moreover, with the selected propulsive parameters, the problem's objective of maximizing the final mass is mostly affected by the thrust time, rather than by the kind of trajectory, hence the optimizer is more prone to reducing the overall maneuver time. All of the identified solutions exhibit a similar structure: when the objective is to raise the orbit, a first phase in which the thrust vector is oriented along the direction of the velocity, with a radial component, is followed by a second circularizing phase in which thrust is provided against the velocity, vice versa happens in the case of an orbit lowering. Fig. 9. and Fig. 10. graphs highlight the fundamental symmetry between the identified orbit raising and orbit lowering solutions:

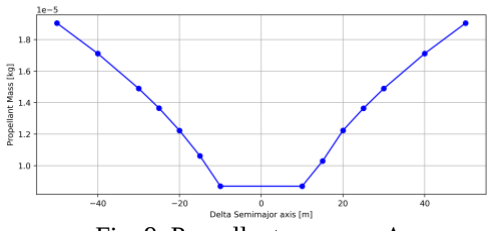

Fig. 9. Propellant mass vs. Δa

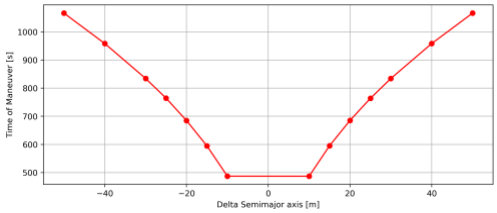

Fig. 10. Time to maneuver vs. Δa

In light of these results, it can be reasonably concluded that the repositioning maneuver to be performed following TCA should bear a strong resemblance to the CAM in terms of propellant expenditure and time to maneuver.

6.4 Initial Costates

Although lacking a physical significance and a clear predictable trend, initial costates can provide valuable insights into a solution's behavior. With experience and critical analysis of the results, sensible guesses can be made. By recognizing that a typical Hohmann-like maneuver has a thrust-coast-thrust structure (TCT), it can be deduced that the initial switching function should be positive. A relationship between the primer vector and the mass costate is established by the definition of the SF (5.9) and is evident in the graph above: when the primer vector rises in module, the mass costate plummets, and vice versa. From the definition of the thrust angles in terms of velocity costates (5.7), it is possible to predict the former if the direction of the initial thrust is known: as mentioned above, the identified trajectories have predictable along-track, along-velocity or against-velocity initial thrust and figure 11 confirms the trend in terms of positive or negative initial velocity costates. Although with a different scale, which is here omitted since it is determined by the problem's optional adimensionalization, the initial position costates follow an almost identical trend compared to the velocity ones. It is important to notice how the dominant costate is related to the x-coordinate, as the primary spacecraft's initial position in the J2000 RF is almost coincident with the x axis. Different co-dependencies can be expected with different initial positions. Parametric analyses of converged solutions are of great importance for the comprehension of costate behaviour, and can be of significant assistance with initial guesses, which, under the influence of the specific characteristics of the optimization problem, can considerably impact the convergence capabilities of the presented method.

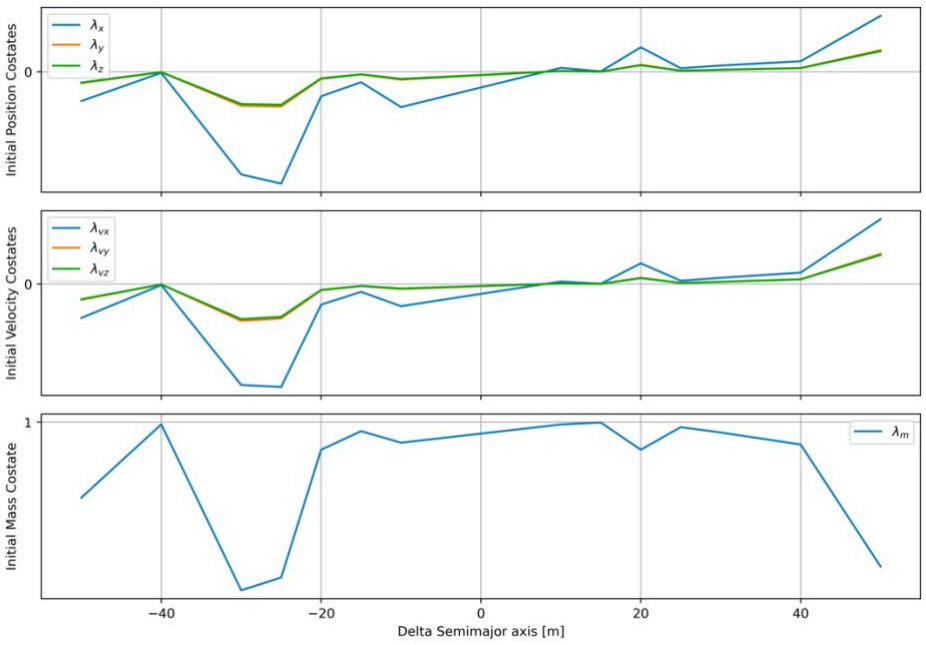

Fig. 11. Initial costates for each solution

7. Closing remarks and future development

The work's objective of developing a fully functional optimization tool based on the indirect transcription of the optimal control problem was widely met. Evasion maneuvers push the boundaries of what can be achieved with indirect methods: the high precision required and the extremely low variation between initial and target states cause convergence to be difficult and obtainable only when initial guesses are good.

By following a homotopy-continuation approach, future developments of the optimization tool should gradually introduce LEO perturbations, and therefore allow for a complete coupling with the PoC computation tool.

Furthermore, the translation of the TPBVP to a Multi-Point BVP with an inequality interior point constraint would guarantee a complete optimization of both the evasion and the re-positioning legs of the CAM, albeit greater problem complexity and convergence difficulties are to be expected.

References

[1] Alessandro Zavoli. .Indirect Optimization of Bang-Bang Control Problems and Applications to Formation Flying Missions.. PhD thesis. Torino: Sapienza, Università di Roma, May 2013. url: https://iris.uniroma1.it/retrieve/e3835315-d387-15e8-e053-a505fe0a3de9/Alessandro%20Zavoli%20-%20PhD%20thesis%20-%20Ciclo%20XXV%20-%20padis.pdf

[2] Yu-Chi Ho Arthur E. Bryson Jr. Applied Optimal Control. 1025 Vermont Ave. N.W., Washington, D.C. 20005: Hemisphere Publishing Corporation, 1975.

[3] Jànos D. Pintér Giorgio Fasano. Modeling and Optimization in Space Engineering.
Springer New York Heidelberg Dordrecht London: Springer, 2013

[4] L.S. Pontryagin. The mathematocal theory of optimal processes, International series of monographs in pure and applied mathematics Pergamon Press book. Pergamon Press; [distributed in the Western Hemisphere by Macmillan, New York], 1964

[5] Luigi Mascolo. .Low-Thrust Optimal Escape Trajectories from Lagrangian Points and Quasi-Periodic Orbits in a High-Fidelity Model.. PhD thesis. Torino: Politecnico di Torino, 2023. url: https://iris.polito.it/handle/11583/2976595

[6] P. Lu B. Pan Z. Chen. .Reduced Transversality Conditions in Optimal Space Trajectories.. In: Journal of guidance, control, and dynamics 36 (Sept. 2013). doi: 10.2514/1.60181

[7] V. Braun K. Merz B. Bastida Virgili. .Current Collision Avoidance service by ESA's Space Debris Office. In: (June 2017)